Phase Diagram and Glass Transition of Confined Benzene

Yongde Xia,† Gilberte Dosseh,* Denis Morineau,‡ and Christiane Alba-Simionesco

Laboratoire de Chimie Physique, UMR CNRS 8000, Université de Paris Sud, Bâtiment 349, 91405 Orsay Cedex, France

Received: June 1, 2006; In Final Form: July 8, 2006

We used differential scanning calorimetry, neutron scattering, and proton NMR to investigate the phase behavior, the structure, and the dynamics of benzene confined in a series of cylindrical mesoporous materials MCM-41 and SBA-15 with pore diameters, d, between 2.4 and 14 nm. With this multitechnique approach, it was possible to determine the structure and, for the first time to our knowledge, the density of confined benzene as a function of temperature and pore size. Under standard cooling rates, benzene partially crystallizes in SBA-15 matrixes ($4.7 \leq d \leq 14$ nm) but not in MCM-41 ($2.4 \leq d \leq 3.5$ nm). Structure factors of the confined phases were recorded at different temperatures and compare to those of the bulk. The confined liquid has the same structure as the bulk above the bulk melting point. In SBA-15, the confined crystals are defective and have the same structure as the bulk. In MCM-41, the liquid undergoes a glass transition at low temperature regardless of the cooling rate or the thermal history of the sample. The density as a function of temperature was measured by neutron scattering contrast matching, and the glass transition temperatures were determined from the density versus temperature curves. The pore size dependence of T_g does not show any evidence of finite size effects. A temperature versus pore diameter phase diagram of confined benzene is proposed combining liquid, supercooled liquid, crystal states, and glassy states. NMR relaxation time measurements showed that the dynamics of the confined liquids are slower than those of the bulk above its melting point. In the partially crystallized samples, the liquid and the crystal have the same relaxation times. The activation energies of reorientation motions in the confined phases, determined from spin lattice relaxation times, are smaller than the bulk ones.

I. Introduction

Properties of fluids confined at the molecular scale are of interest in many fields because of their importance in a variety of technological processes including catalysis, membrane separation, chromatography, lubrication, fabrication of nanomaterials, and nanotribology. Among the issues that are still being addressed are the following: How can phases and their transition be defined at the nanoscale? What is the influence of the properties of the confining media (pore size, dimensionality, connectivity, and surface properties) on the behavior of the confined phases? In recent years, a considerable amount of progress in understanding the thermal and dynamical properties of molecular liquids in rigid confinement has been made, as reported in several reviews and references therein.[1−6] The phenomenology of freezing and melting of organic compounds in hard confinement (silica- or carbon-walled porous materials, zeolites, etc.) has been widely investigated.[4−12] The melting point is usually shifted of ΔT ($\Delta T = T_{conf} - T_{bulk}$) with respect to the bulk. In the most studied porous materials, ΔT is negative, and the shift increases with decreasing pore size. The main factors that influence the melting parameters are the ratio between the pore diameter d and the van der Waals diameter of the confined fluid, σ_{vdW}, $H^* = d/\sigma_{vdW}$, fluid−wall interactions, and the geometry of the confining media.[10,12] When the confined fluid and the porous materials have weak Lennard-Jones-type interactions, ΔT follows the Gibbs−Thomson equation for large pores (roughly $d > 20\ \sigma_{vdW}$). In small pores ($d < 10\ \sigma_{vdW}$), crystallization is usually not observed, and the confined liquid undergoes a glass transition at low temperature. Between these limits, the confined liquids partially crystallize, and the melting temperature dependence on the pore size fails to follow the Gibbs−Thomson equation.[12] The departure from the Gibbs−Thomson equation and the possibility to avoid crystallization depend on the properties of both the adsorbed fluid and the porous materials.[12] Benzene confined in silica-walled MCM-41 does not crystallize in pores with diameters smaller than $\sim 10\ \sigma_{vdW}$ but undergoes a glass transition at common cooling rates (less than 10 K.min^{-1}), whereas bulk benzene usually crystallizes at these cooling rates. The first experimental observation of a glass transition of benzene in a differential scanning calorimetry (DSC) experiment was reported by Dubochet et al. They measured a glass transition temperature of 118 K for benzene confined in microemulsion with pore size of around 20 nm.[14] In rigid-walled SBA-15 materials ($10 < d < 18\ \sigma_{vdW}$), the melting temperature of confined benzene does not follow the Gibbs−Thomson equation, whereas water confined in the same materials crystallizes in $8\ \sigma_{vdW}$ pores and follows the Gibbs−Thomson equation for pore sizes larger than $8\ \sigma_{vdW}$.[12,13] Fluid−wall interaction is one of the main parameters that influence the sign of ΔT. When the adsorbed fluid and the confining media have weak attractive or repulsive interactions, the melting point decreases. On the other hand, strong fluid−wall interactions can lead to an increase of melting temperature

* E-mail: Gilberte.Dosseh@lcp.u-psud.fr. Also at Département de Chimie, Université de Cergy − Pontoise, mail Gay-Lussac F-95031 Neuville Sur Oise, France.

† Present address: B11, School of chemistry, The University of Nottingham, University Park, Nottingham NG7 2RD, United Kingdom.

‡ Present address: Groupe Matière Condensée et Matériaux, Bât. 11A, Université de Rennes, F-35042 Rennes, France.

10.1021/jp063393i CCC: $33.50
Published on Web 09/12/2006

as observed by Kaneko and colleagues for benzene confined in activated carbon fibers (ACF).[15] Strongly attractive walls may also induce the appearance of new surface-driven phases such as the hexatic phase observed for nitrobenzene adsorbed in MCM-41.[16] The shape of the pores is another parameter of importance as illustrated by experiments on surface force apparatus.[17−22] Molecular liquids confined between mica parallel plates experienced an increase of the freezing point. For example, cyclohexane confined between mica plates froze 17 deg above the bulk melting point for an interplane distance of 7 molecular diameters.[22]

The possibility of avoiding crystallization by confining liquids in small pores has introduced the opportunity to study new phenomena such as supercooling over a large temperature range and vitrification in systems which usually do not vitrify in common experimental conditions. Besides studies on phase transitions, considerable work was initiated to understand the structure, the thermodynamics, and the dynamics of confined phases by the means of various experimental techniques. Modifications in the confined-phase properties are difficult to extract using common experimental methods. Going forward and backward between experiments and simulations can be helpful for the understanding of experimental data.[23,24] Another important issue is the precise knowledge of the thermodynamic state of the confined phase and of the paths followed during the transitions. The phase composition of confined systems is also of concern. Numerous experiments have shown that, when fluid−wall interactions are repulsive or weakly attractive, crystallization is often partial, and a liquid or glassy layer may persist at very low temperature at the surface of the pores.[12,25−27] The smaller the pore size, the thicker the liquid layer is, and the broader the melting transition is. In large pores, crystallization may be complete. For cyclohexane confined in CPG, crystallization is completed below 250 K in pores of 20 nm ($\sim$40 σ_{vdW}) and below 268 K in pores of 50 nm ($\sim$100 σ_{vdW}).[25] The first indication of a decrease in density in a liquid under confinement was provided by Morineau et al. who used contrast matching neutron scattering experiments to determine the density of confined toluene.[28] They showed that toluene confined in pores smaller than 8 molecular sizes has lower density than bulk toluene at the same temperatures. The presence of a wall and adsorbate−adsorbent interactions induce a slowdown of the molecules in contact, leading to heterogeneous dynamics in the system, as shown in molecular dynamics simulation of toluene confined in pores with frozen toluene walls or different experimental methods such as NMR, dielectric spectroscopy, neutron time-of-flight, neutron spin−echo, or optical Kerr effect.[29−34] Richert and Min studied supercooled 3-methylpentane confined in 7.5-nm porous silica by triplet-state solvation dynamics.[35] The dynamics of the liquid layer close to the wall is 3 orders of magnitude slower than those of the bulk at the same temperature and almost 2 orders of magnitude slower than the average dynamics of the liquid inside the pore.

The challenge now is to overcome the experimental difficulties in order to disentangle the effects that are implicated in the behavior of confined phases. New synthesis methods have introduced the possibility of tailoring porous materials with desired properties. They allow the fabrication of ordered materials with various surface properties. The topology of the porous materials (pore shape and connectivity) can be kept constant, while the surface properties are modified, allowing the investigation of fluid−wall interaction effects on phase transitions at the nanoscale. Confinement of model compounds such as benzene in model matrixes (for instance, single cylindrical silica-walled pores such as MCM-41, SBA-15, or slit pores) can be helpful for a better understanding of the phenomenology of the behavior of confined phases. We chose to study benzene because its structure is simple and well-known. The bulk phases have been extensively studied. Molecular simulation of the dynamical and structural properties of bulk benzene have also been carried out.[36] Comparison of the properties of confined benzene with those of the bulk can be made easily, and molecular simulation of confined benzene can be performed using the usual simulation methods. Understanding the phenomena that occur in such a compound under confinement could be the beginning of systematic studies of a confined system with increasing complexity. In a previous paper, we examined the effects of confinement on freezing and melting of benzene in silica-walled highly ordered mesoporous materials MCM-41 ($2.4 < d < 3.6$ nm) and SBA-15 ($4.7 < d < 14$ nm).[12] Benzene confined in SBA-15 materials crystallizes but does not in MCM-41 materials. An analysis of the melting point depression in terms of the Gibbs−Thomson equation and comparisons with both water confined in the same matrixes and the results of Jackson and McKenna for benzene confined in sylanized CPG showed that the agreement with the Gibbs−Thomson equation depends on the interactions between the confined molecules and the pore walls.[7,12] The broadening of the transition, similar for SBA-15 and sylanized CPG materials, not only depends on the pore size distribution but may also be imputed to a progressive layer-by-layer melting of the confined crystals. The smaller the pore, the broader the temperature range of the transition is. Proton NMR line-shape analysis showed that benzene confined in SBA-15 ($4.7 \leq d \leq 8.7$ nm) always crystallizes partially in the temperature range under study ($153 \leq T \leq 300$ K). In MCM-41, crystallization is always avoided even at cooling rates as low as 2 K.min^{-1}, and the confined liquid undergoes a glass transition, while the bulk one usually crystallizes at these cooling rates. A first phase diagram of confined benzene, displaying the melting temperature versus pore size, was proposed.

We focus here on a more general phase diagram of the condensed phases of confined benzene. The purpose is to complete the phase diagram of confined benzene and to investigate the effects of pore size and surface interactions on melting and glass transition. We also investigated effects of confinement on the structural and dynamical properties of benzene by means of calorimetry, neutron scattering, and proton NMR experiments. Our aim is to get a better knowledge of the thermodynamical state of the adsorbate. We present here the first measurements of the density of confined benzene by the means of small-angle neutron scattering. Its temperature dependence defines the thermodynamical path followed during the transitions. The transition temperatures were determined at the maximum of the DSC peak, and NMR line shape analysis provided the composition of the samples. In addition to DSC and NMR, the local structure of the confined phases was studied by elastic neutron scattering. Finally, we investigated the dynamical properties of confined benzene by looking into evolution of the NMR line widths, the spin−spin relaxation, and the spin−lattice relaxation times.

The occurrence of a glass transition in a simple liquid like benzene, which does not vitrify at common cooling rates in the bulk, provides the possibility of testing the models of the glass transition. In particular, the existence of a correlation length associated with the glass transition will be examined. Comparison with fragile glass-forming toluene confined in the same materials may provide an insight of how benzene could be

TABLE 1: Structural Parameters of Mesoporous Silicates MCM-41 and SBA-15

sample	surface area (m^2/g)	pore volume (cm^3/g)	pore size (nm)
MCM-41-C10	960	0.43	2.4
MCM-41-C16	724	0.57	3.5
SBA-15A	560	0.67	4.7
SBA-15B	770	1.21	6.8
SBA-15C	690	1.34	8.7
SBA-15D	440	1.63	14.0

considered with respect to usual glass-forming liquids in the Angell classification.

II. Experimental Methods

II. 1. Synthesis and Characterization of the Mesoporous Materials. MCM-41 materials were prepared in our laboratory according to a modified procedure described by Grün and coworkers.[37] The detailed procedure was reported in a previous paper.[38] Hexadecyl trimethylammonium bromide and decyl trimethylammonium bromide were used as cationic surfactants and tetraethoxysilane (TEOS) as a silica source. The synthesized mesoporous materials were labeled MCM-41-C16 and MCM-41-C10. The SBA-15 samples were synthesized as reported by Zhao et al.[39] Triblock copolymer Pluronic P123 ($EO_{20}PO_{70}EO_{20}$) was used as a surfactant. By changing the aging temperature from 35 to 100 °C, samples with different pore size from 4.7 to 8.7 nm were obtained. Addition of the organic swelling agent 1,3,5-trimethylbenzene leads to a pore size of 14.0 nm. To remove the surfactants, the as-synthesized MCM-41 and SBA-15 materials were calcinated for 6 h at 823 and 773 K, respectively, in a flow of air.

Structural properties of the synthesized MCM-41 and SBA-15 were investigated using nitrogen adsorption and small-angle neutron scattering measurements.

Adsorption isotherms of both materials were acquired with a Micrometrics ASAP 2010 volumetric adsorption analyzer. The BET surface areas were calculated from data in the relative pressure range from 0.03 to 0.2. Pore diameters of MCM-41 samples, 2.4 and 3.5 nm, respectively, were calculated using a combination of neutron diffraction and nitrogen adsorption, according to the method proposed recently by Kruk et al.[40] For SBA-15 materials, pore diameters of 4.7, 6.8, 8.7, and 14.0 nm were obtained at the maximum of the geometric pore size distributions. The pore size distributions were determined from the adsorption branches of nitrogen isotherms using an algorithm based on the procedure proposed by Barett−Joyner−Halenda.[41]

The structural properties of all the materials are summarized in Table 1.

II. 2. Sample Preparation. Liquid benzene was distilled at reduced pressure before sample preparation.

The bulk benzene samples were sealed under vacuum in the NMR tube in order to avoid contamination with oxygen and water.

To desorb water from the porous materials, the empty matrixes were dried at 150 °C under vacuum for at least 24 h. The volume of liquid that fills the pores was determined by adsorption measurements. The calculated volume was then injected into the sample with a syringe at room temperature. After an equilibration time of a few hours, which allows the liquid to diffuse into the pores, the samples were transferred into NMR tubes or DSC cans and sealed.

II. 3. Evaluation Methods. *II. 3. a. DSC Measurements.* The DSC measurements were performed using a Perkin-Elmer DSC2. A homemade temperature unit was adapted to allow low-temperature measurements (down to 80 K). The temperature calibration was made with the bulk compound. All the samples were slightly overloaded in order to detect the bulk and confined transition temperatures, allowing a precise determination of the temperature depression.

All the scans were carried out at heating or cooling rates of 10 $K.min^{-1}$.

II. 3. b. Neutron Scattering Measurements. Elastic neutron scattering experiments were carried out to study the structure of the adsorbate at the reactor Orphée of the Laboratoire Léon Brillouin (CEA-CNRS, Saclay, France), on three different spectrometers (PAXE, G6-1, 7C2) in order to cover an extended Q-range from 10^{-2} to 10^{1} $Å^{-1}$. The diffraction patterns of the mesoporous matrixes were recorded on the small-angle spectrometers PAXE for SBA-15 and G6-1 for MCM-41 materials with an incident wavelength of 7 Å and a 64 cells × 64 cells XY multidetector.

The high-Q parts of the spectra were obtained on G6-1 and 7C2 at 4.7 and 1.1 Å, respectively. G6-1 and 7C2 are double-axis spectrometers with BF_3 distance-sensitive linear detectors containing, respectively, 400 and 640 cells.

A full standard correction procedure was applied to the experimental diffraction intensities. The detailed procedure was described elsewhere.[42,43] For the structural studies of confined benzene, the contributions from the matrix−matrix correlations were removed by subtraction of a properly weighted spectrum of the empty matrixes.

II. 3. c. NMR Measurements. The ^1H NMR measurements were carried out at 250.13 MHz on a commercial Bruker DPX 250 spectrometer equipped with a Bruker variable temperature controller. The temperature stability is ±1°. The temperature at the sample was calibrated using pure methanol. All the experiments were done while heating at 2 $K.min^{-1}$ with an equilibration delay of 10 min before measurement. Spin−lattice relaxation times T_1 measurements were performed using a standard inversion−recovery $180-\tau-90$ sequence with a recycle time between each scan larger than $5T_1$. Fifteen delays τ were used to determine each T_1. Spin−spin relaxation times T_2 were measured using the Carr−Purcell−Meiboom−Gill sequence. Twenty-five delays τ were used for each T_2 with a recycle time between each scan larger than $5T_1$. The reproducibility of the measurements was within ±5%.

Line-shape analysis performed on ^1H NMR spectra obtained by Fourier transform of free induction decays recorded with 32−128 scans and a recycle delay between to scans of $>5T_1$. The fractions of liquid and solid were calculated using the DMFIT program proposed by Massiot et al.[44] The reproducibility of the calculated values was within ±3%.

III. Results

III. 1. Phase Transitions, Phase Composition, and Structure. Phase behavior of benzene confined in MCM-41 ($2.4 \leq d \leq 3.5$ nm) and SBA-15 ($4.7 \leq d \leq 14.0$ nm) was studied by NMR and DSC between 150 and 300 K.[12] The static structure factor was also measured by neutron diffraction for bulk benzene and benzene confined in MCM-41 ($d = 2.4$ nm) and in SBA-15 ($d = 6.8$ nm) at 290 K (Figure 1). The differences between confined and bulk liquid structure factors are mainly a negative intensity at low Q due to the subtraction of the empty matrice contribution and a decrease in the intensity of the first maximum of the main diffraction peak in confined geometry. Figure 2a depicts structure factors of bulk benzene and benzene confined in MCM-41 and SBA-15 at 70 K. At this temperature, the structure factor of benzene confined in SBA-15 reflects the

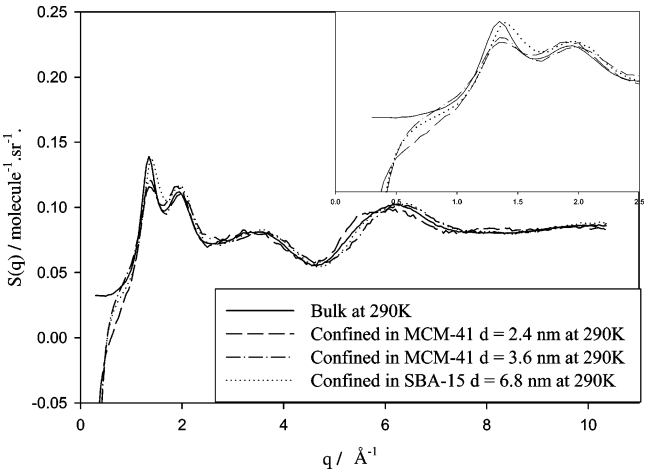

Figure 1. Static structure factors of bulk and confined benzene at 290 K. The insert represents the structure factors in the 0−2.5 Å^{-1} range.

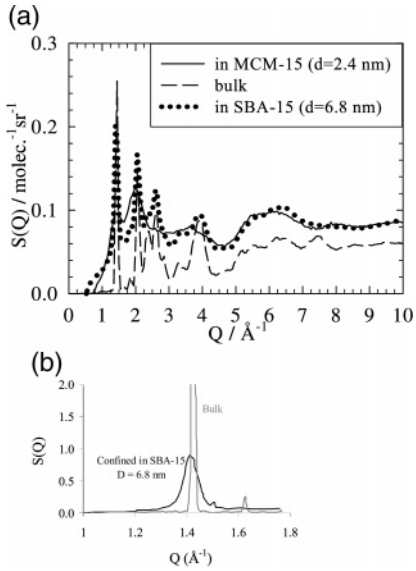

Figure 2. Static structure factors of bulk and confined benzene at 70 K. (a) Comparison of the structure factors of bulk benzene and confined benzene. (b) Comparison of the Bragg peaks of bulk and confined benzene at a better resolution.

presence of a crystalline phase, whereas benzene confined in MCM-41 is amorphous. Bulk and confined crystals have the same symmetries, but the Bragg peaks are broadened for the confined crystal due to the cutoff of the pores (Figure 2b). A similar broadening was also observed for confined smectic liquid crystals where finite size effects are clearly identified.[45] Proton NMR spectra showed that crystallization of benzene confined in SBA-15 is partial (Figure 3a). The two-phase NMR spectra of confined benzene show a broad Gaussian line of ∼12 kHz characteristic of a crystal with reorienting molecules and a narrow Lorentzian line due to the liquidlike molecules. Unlike water, the melting point depression does not follow the Gibbs−Thomson equation in the pore size range under study. Previous experiments reported in the literature show that, even if benzene does not have a dipole moment and cannot form hydrogen bonds, it strongly wets silica (the contact angle of benzene on silica is about 6°).[46] However, the pore size dependence of the melting point depression shows that interactions of benzene with the silica walls are less strong than those of water, which can form hydrogen bonds with silica. In SBA-15, the amount of liquid as a function of temperature, calculated from the ^{1}H NMR spectra, decreases with temperature and seems constant below

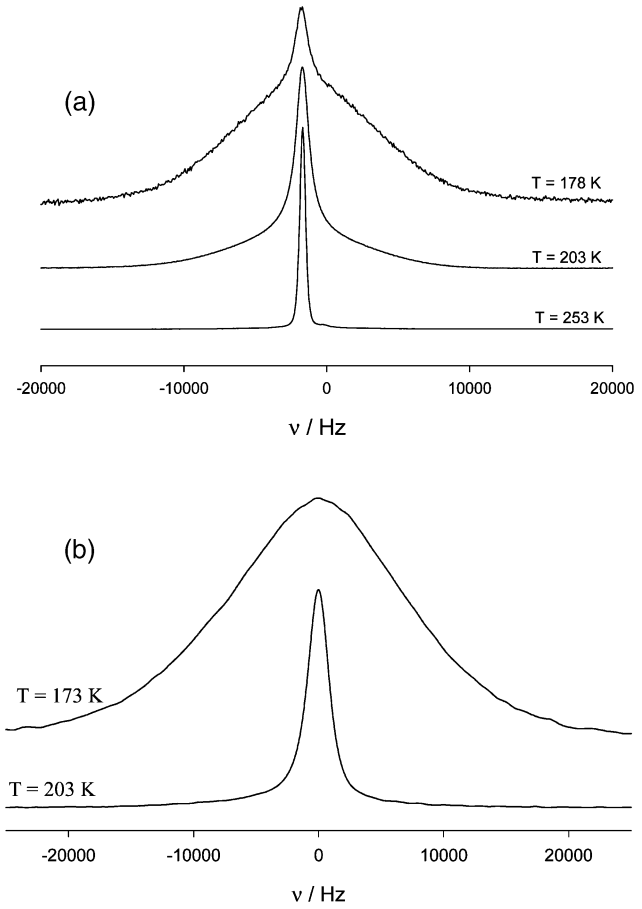

Figure 3. Melting and glass transition in confined benzene by proton NMR. (a) Benzene confined in SBA-15 (d = 4.7 nm) shows partial crystallization at low temperature. The broad line represents the crystal and the thin line the liquid. (b) Benzene confined in MCM-41 (d = 3.5 nm). The liquid vitrifies at low temperature.

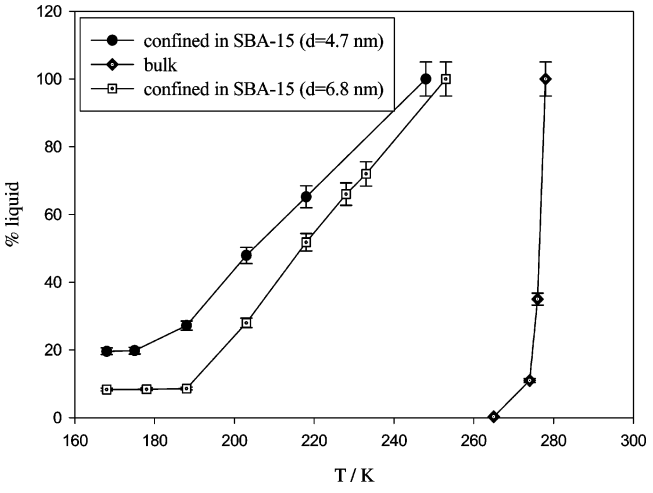

Figure 4. Melting of liquid in bulk benzene and benzene confined in SBA-15. Fraction of liquid as a function of temperature.

173 K for d = 4.7 nm and below 188 K for d = 6.8 nm (Figure 4).[12] The smaller the pore size, the larger the amount of liquid is at a given temperature. At 168 K, the amount of liquidlike molecules are, respectively, 19.6% in the pore of 4.7 nm and 8.3% in those of 6.8 nm (Figure 4). These results are in agreement with those of Gedat et al. who used deuterium NMR to study benzene confined in 8.0 nm SBA-15 from 19 to 236 K. They observed a liquidlike line superimposed over a solid line down to 154 K.[47] We did not record spectra at temperatures

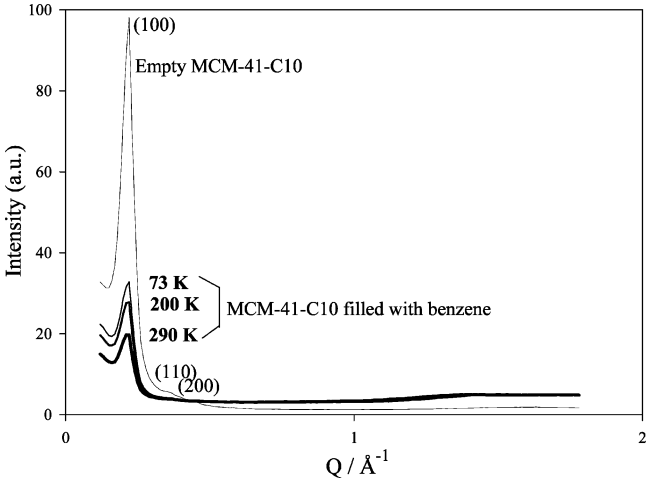

Figure 5. Temperature dependence of the Bragg peaks of empty and filled MCM-41 ($d = 2.4$ nm) as measured on the G6.1 spectrometer (LLB, France).

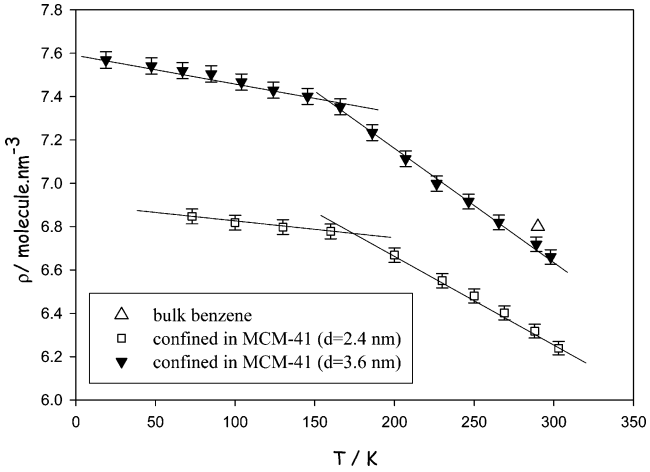

Figure 6. Density of confined benzene as a function of temperature.

TABLE 2: Glass Transition of Confined Benzene

sample	pore size (nm)	T_g/K
microemulsion	20	118 ± 5
MCM-41	3.5	155 ± 5
MCM-41	2.4	170 ± 5

TABLE 3

d/nm	2.4	3.5	4.7	6.8	bulk
line width $\Delta\nu$/Hz	520 ± 1	432 ± 1	416 ± 1	320 ± 1	5.0 ± 0.2
T_2/ms	17 ± 2	23 ± 3	24 ± 3	30 ± 3	620 ± 3

lower than 150 K, but Gedat et al. showed that a transition to a rigid solid, where the reorientation motions are frozen, occurs below 100 K in their sample.

The proton NMR spectra displayed in Figure 3b show that, in MCM-41 ($d = 2.4$ and 3.5 nm), benzene does not crystallize on cooling. The line remains Lorentzian down to 185 K. Below this temperature, the line width increases from a few hundreds of Hertz to 12 kHz and remains constant down to 150 K. The evolution of the line width reflects a slowdown of the molecular motion. The line becomes Gaussian when the molecular motion is slower than the experimental time scale. On heating, no composite line appears, but the line decreases sharply. We interpret this behavior as the signature of a glass transition. Even though these results are an indication of a glass transition, a quantitative determination of the calorimetric glass transition temperature needs other experiments. Glass transition temperatures are usually determined via viscosity ($\eta = 10^{13}$ poise), dielectric (structural relaxation time $\tau = 100$ s), or calorimetry measurements (structural relaxation time $\tau = 200$ s in DSC or 1000 s in adiabatic calorimetry). The signature of a glass transition appears in calorimetric measurements as a jump in the specific heat C_p or in the thermal expansion α of the system or as a change of slope in the temperature versus density curve. Because of the very small amount of liquid inside the pores, we could not observe a glass transition of confined benzene in the DSC scans. We used small-angle neutron scattering to determine the density of benzene confined in MCM-41. For a sample made of a molecular liquid confined in an ordered mesoporous material, scattering at small angles or small momentum transfer ($Q < 0.3$ Å^{-1}) is due to the hexagonal arrangement of the cylindrical pores. The intensity I of the main diffraction peak depends on the contrast. The contrast is defined as the square of the scattering length density difference between the matrix and the confined liquid. The intensity of the matrix main diffraction peak is given by

$$I = A(\rho_{SiO_2}\overline{b_{SiO_2}} - \rho_{liq}\overline{b_{liq}})^2$$

where $\rho_{SiO_2}\overline{b_{SiO_2}}$ and $\rho_{liq}\overline{b_{liq}}$ are the scattering length densities of silica and the confined liquid, respectively, and A is a constant. Figure 5 shows Bragg peaks (100, 110, 200) of the empty matrix and the filled matrix at several temperatures. By comparing the intensities of the (100) peaks of the empty matrix with those of the filled matrix at a given temperature, and assuming that the density of the matrix wall is the same as that of amorphous silica at atmospheric pressure (2.2 g.cm^{-3}), the density of the confined phases was determined as a function of temperature (Figure 6). At 290 K, above the bulk melting point, the density of confined benzene is always smaller than that of the bulk. The smaller the pore, the lower the density is. We could not compare the bulk and confined liquid densities at temperatures lower than the bulk melting point, because benzene always crystallizes in our experimental conditions. However, the same experiments on confined toluene showed that the difference between the densities of bulk and confined toluene increases with decreasing temperature, showing that the expansivity of the confined liquid is smaller than that of the bulk.[28] Table 2 gives the glass transition temperatures of benzene confined in MCM-41. T_g increases with decreasing pore size in MCM-41 pores. On heating, the glass transition is never followed by crystallization and melting, as observed for benzene confined in microemulsion.[14]

III. 2. Dynamics. *III. 2. a. Proton NMR Line Widths and Spin−Spin Relaxation Times.* In proton NMR, the dominant anisotropic term in the spin Hamiltonian is the dipolar coupling between all protons in the system. In a rigid crystal, no interaction is averaged, and the static line width is usually on the order of tens of kilohertz. The occurrence of molecular motions gives rise to a decrease of the line width. Molecular reorientations partially average out dipolar interactions and lead to a line width of about 10−15 kHz. In a bulk liquid, molecules experience reorientation and self-diffusion motions. Intra- and intermolecular dipolar interactions are averaged out, leading usually to a Lorentzian proton line of a few hertz. At 298 K, the bulk liquid benzene line has a width of 5 Hz after shimming on our spectrometer. The line widths of confined liquid benzene are 2 orders of magnitude larger than the line width of the bulk at 298 K (Table 3). The broadening of the line in confined geometry can be explained by two concomitant factors. One is the field inhomogeneities introduced by the differences in

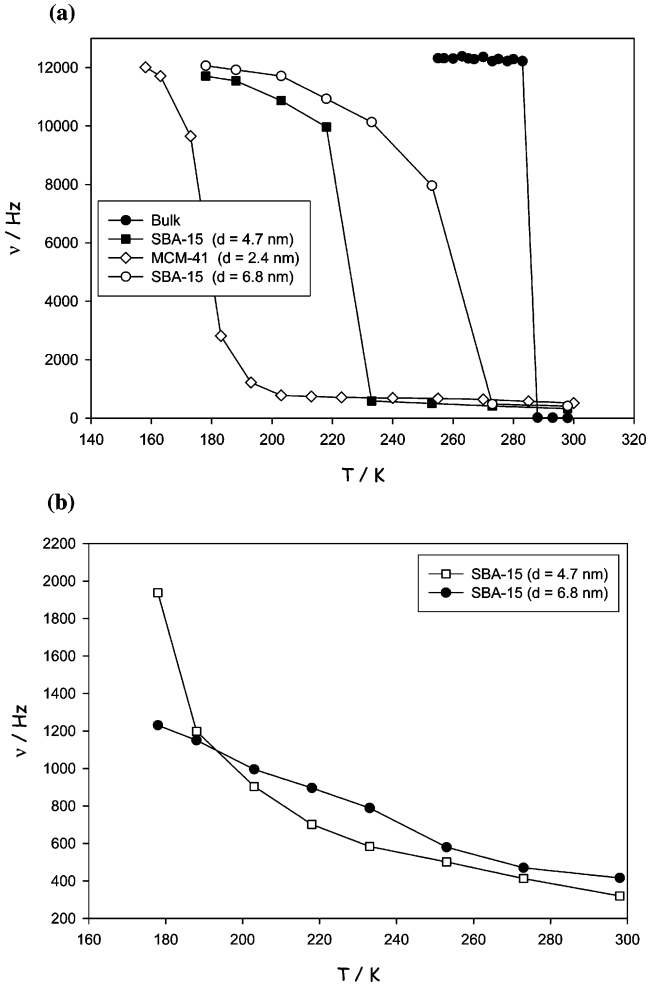

Figure 7. (a) Proton NMR line width of bulk and confined benzene as a function of temperature showing the melting transition (for bulk benzene and benzene confined in SBA-15) or the glass transition (for benzene confined in MCM-41). (b) Proton NMR line width of the liquidlike line in the two-phase samples. The line is 2 orders of magnitude larger than those of the bulk liquid.

magnetic susceptibilities between the pore walls and the confined fluid. The other one is a slowdown of the dynamics due, on one hand, to the presence of a rigid wall and, on the other hand, to surface interactions between the pore walls and the confined fluid. For a Lorentzian line, the experimental line width is related to the spin−spin relaxation time T_2 through the expression $\Delta\nu = 1/T_2 + \gamma\Delta B$ where γ is the gyromagnetic ratio and ΔB represents the field inhomogeneity. The spin−spin relaxation times at 298 K given in Table 3 showed that the broadening of the line of confined benzene is due not only to internal field inhomogeneities but also to a slowdown of the molecular motions. In a liquid, when molecular motions are fast, the spin−spin relaxation rate $R_2 = 1/T_2$ is proportional to the molecular motion correlation time τ_c. A slowdown of the molecular motions due to confinement effects leads to a decrease of T_2 with pore size.

The line widths as a function of temperature are presented in Figure 7 for confined and bulk samples. For partially crystallized samples (benzene confined in SBA-15), the widths of the crystal (Figure 7a) and the liquidlike sample (Figure 7b) are displayed. The line width of the crystals reaches the value of 12 kHz and remains constant at low temperature, showing a reorienting crystal as bulk benzene (Figure 7a). The width of the liquidlike line increases with decreasing temperature showing a progressive slowdown of the translational motions (Figure 7b). Benzene

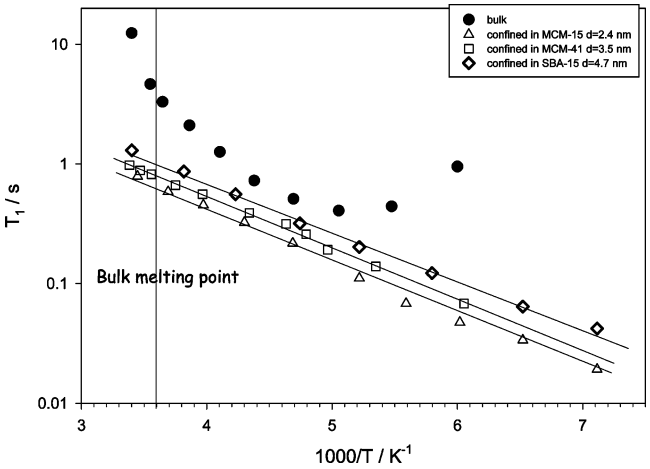

Figure 8. Proton spin−lattice relaxation times as a function of the reverse temperature. The vertical line corresponds to the melting temperature of bulk benzene. The relative error is 5%.

confined in MCM-41 exhibits a single line whose width increases with decreasing temperature (Figures 3 and 7a), showing a progressive slowdown of the dynamics in the whole temperature range we studied.

III. 2. b. Spin−Lattice Relaxation Times. Spin−lattice relaxation times T_1 of bulk and confined benzene were measured at several temperatures. Figure 8 presents semilogarithmic plots of spin−lattice relaxation rates $1/T_1$ versus reciprocal temperature for bulk and confined benzene. In bulk benzene, a discontinuity appears in the T_1 versus $1/T$ curve at the melting point represented by the vertical line. In the bulk crystalline phase, T_1 versus $1/T$ shows a minimum characteristic of the Bloembergen, Purcell, and Pound (BPP) theory.[49] The data have been fitted using the Kubo and Tomita weak collision theory.[50] In this theory, the relaxation rate can be written as $1/T_1 = C[\tau_c/(1 + \omega_0^2\tau^2) + 4\tau_c/(1 + 4\omega_0^2\tau_c^2)]$ where τ_c is the correlation time of the motion responsible for the spin lattice relaxation, ω_0 the resonance frequency of the nuclei, and C a constant. $1/T_1 = f(1/T)$ has a maximum for $\omega_0\tau_c = 0.616$, leading to a correlation time of 3.9×10^{-10} s at $T(T_{1\min}) = 213$ K for the molecular motion. Assuming that τ_c follows an Arrhenius type law, we have determined an activation energy of 15.5 kJ.mol^{-1}, in agreement with values published in the literature.[47]

For confined benzene, an average spin−lattice relaxation time was measured at each temperature. The supercooled liquid and the crystal have the same spin−lattice relaxation times as depicted in Figure 9, where the evolution of the magnetization of the liquid and the solid as a function of the inversion recovery τ delays is plotted at 200 K. In confined benzene, the average relaxation times are always smaller than in the bulk, indicating an increase of molecular motion correlation times due to a strong restriction of reorientation and translation motions. These results are in agreement with the results of Jonas and Yi and those of Zhu et al. who studied benzene confined in silica-walled porous materials and reported strong restrictions in molecular motions of the confined liquid.[46,51] The enhancement of relaxation rates increases with decreasing pore sizes as usually observed in confined liquids.[49] No discontinuity appears in the T_1 versus temperature curve at the melting point for the partially crystallized sample (benzene confined in SBA-15). The relaxation rate decreases with temperature, and its logarithm is a linear function of the reverse temperature, following an Arrhenius-type law. This evolution suggests that, in the whole temperature range, $\omega_0\tau_c \ll 1$ and $1/T_1$ is proportional to τ_c. All the confined samples have activation energies of about 8 kJ.mol^{-1} (Table 4).

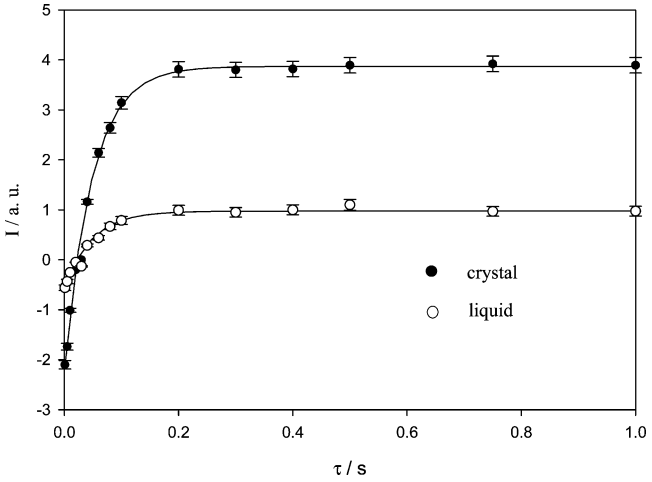

Figure 9. Evolution of the line intensity of the NMR line in an inversion recovery experiment as a function of the delay τ.

IV. Discussion

IV. 1. Phase Composition and Phase Diagram. *IV. 1. a. Structural Properties of the Liquid.* The interpretation of the structural properties of confined benzene is difficult. To determine the origin of the changes in the structure factor under confinement, calculations of the structure of liquid benzene confined in cylindrical pores were carried out by Morineau and Alba-Simionesco. The calculation methods and detailed results were reported previously.[43] They showed that these differences are mainly due to two effects that do not exist in the bulk but are present in confined geometry. One is the so-called excluded volume effect. It arises from the fact that a fraction of space (occupied by the matrix) is not accessible for the liquid molecules. The second effect is due to the mixing of liquid−liquid and liquid−matrix correlation terms in the structure factor. The experimental structure factor is a superposition of three contributions: fluid−fluid correlation terms, matrix−matrix correlation terms, and cross-correlation terms. A simple subtraction of the properly weighted empty matrix cancels the matrix−matrix correlations terms but not the cross-terms. These results showed that the distortions appearing on the static structure factor of confined liquid benzene at 290 K do not reflect a change in local ordering due to confinement but is mainly due to excluded volume effects.

IV. 1. b. Crystallization and Melting. The proton NMR line shapes presented in section III. 1 show that, in the whole temperature range, benzene confined in SBA-15 forms a two-phase system. The line widths of the bulk and confined crystals are equal. Moreover, the structure factors show that both bulk and confined benzene crystals have identical structures. The only difference between them is the broadening of the peak of confined crystals. This broadening can be attributed to the decrease of the crystallite size upon confinement and the formation of a defective crystal. Assuming that the crystallites are located at the center of the pores and the liquid at their surface, as suggested by Monte Carlo simulation of Gubbins and colleagues,[11] the thickness of the liquid layer at the surface is $a = (d_{pore} - d_{crystal})/2$. Knowing the expression of the fraction of crystal in the sample

$$x_c = \frac{V_{crystal}}{V_{pore}} = \left(\frac{\pi \frac{d_{crystal}^2}{4} h_{pore}}{\pi \frac{d_{pore}^2}{4} h_{pore}} \right)$$

TABLE 4: Reorientation Activation Energy for Bulk and Confined Benzene

d/nm	2.4	3.5	4.7	6.8	bulk
E_a/kJ.mol^{-1}	8.6 ± 0.4	7.7 ± 0.5	8.2 ± 0.5	7.9 ± 0.5	15.5 ± 1.0

we can calculate a as $a = {}^1/_2\, d_{pore}(1 - \sqrt{x_c})$. The calculated thicknesses at 168 K, 4.4 Å in the 4.7 nm pores and 3.0 Å in the 6.8 nm pores, are less than the diameter of a benzene molecule (5 Å). These values can be interpreted in two ways: (1) The benzene cycles are preferably parallel to the wall in a position which favors the interaction between the π electrons of the benzene cycles and the hydrogen of the hydroxyl function at the surface of the pores. It is then difficult to determine the number of liquid layers in each sample. This interpretation is in agreement with the results of Zhu et al., who showed that benzene molecules lie parallel to the wall, with an interfacial layer thickness of 2.5 Å or less, when they are confined in nanoporous silica.[46] (2) A part of the liquidlike surface layer has vitrified at this temperature. The crystalline phase of benzene has an orthorhombic symmetry with lattice parameters $a = 7.460$ Å, $b = 9.666$ Å, and $c = 7.034$ Å.[52] Assuming that the diameter of the cylinder available for the crystals is $4.70 - 2 \times 0.44 = 3.82$ nm in the 4.7-nm pores, we can see that a crystal can exist in a cylinder whose diameter is 4 times the larger size and 5.4 times the smallest size of the cell. On the other hand, the largest pore size of MCM-41 used in our experiments (3.5 nm) corresponds to 3.7 times the largest size and 5 times the smallest size of the lattice cell. Considering that the thickness of the liquid layer is larger than in the 4.7-nm SBA-15, the diameter of the cylinder available for the crystal would be less than 2.7 nm. This means that the liquid does not crystallize if the diameter of the cylinder is less than 2.8 times the larger size and 3.8 times the smallest size of the lattice cell. Kaneko and Watanabe showed that benzene confined in activated carbon fibers (ACF) crystallizes in pores as small as 0.75 nm.[15] However, direct comparisons of our results with those of Kaneko is not possible, because in ACFs, the phases are confined in one dimension, whereas they are confined in 2 dimensions in cylindrical pores. More experiment are needed to separate the respective parts of pore topology and fluid−wall interactions in the behavior of confined phases. Changing pore topology for given fluid−wall interactions would provide information on the role of the pore topology on the melting properties of confined fluids. Modifications of the surface properties of the porous materials while keeping the same topology would help to understand fluid−wall interaction effects.

We have shown in a previous section that benzene confined in SBA-15 ($4.7 \leq d \leq 14$ nm) does not follow the Gibbs−Thomson equation.[12] This may be caused by the decrease of the density of the liquid inside the pore. It may also come from the fact that the liquid layer at the surface of the pores changes the diameter of the pores that should be used in the Gibbs−Thomson equation.

IV. 1. c. Glass Transition. The glass transition is usually detected experimentally with different methods. DSC and dielectric spectroscopy are the most common methods used to determine glass transition for $\tau = 200$ s and 100 s, respectively. NMR line shape analysis may also be used to detect glass transition from the line shape dependence on temperature. However, the time scales probed by these methods differ by several orders of magnitude. The correlation times of the motions responsible for the line narrowing on heating can be determined at the onset of the line width jump. The correlation times are equal to the reciprocal of the Gaussian line width (here, ~0.1 ms). As the glass transition determined by DSC and

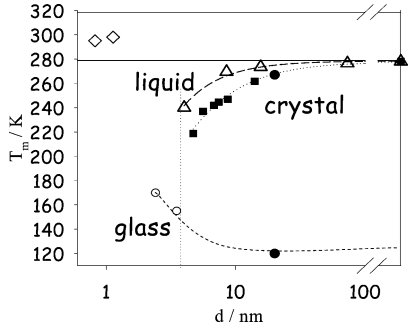

Figure 10. (*d*, *T*) Phase diagram of confined benzene: (■) melting point of benzene confined in hydroxylated SBA-15; (△) melting point of benzene confined in sylanized CPG (ref 53); (◇) melting point of benzene confined in ACF (ref 15); (○) glass transition temperature of benzene confined in MCM-41; (●) glass transition and melting temperatures of benzene confined in microemulsion.

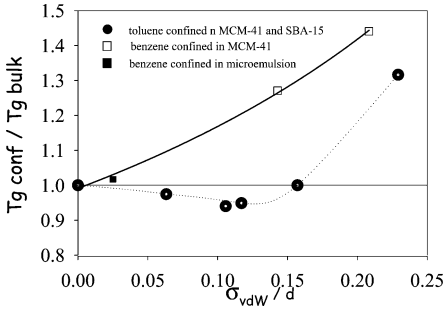

Figure 11. Glass transition temperatures of confined benzene and toluene as a function of the normalized reverse pore size (σ_{vdW}/d) with X (benzene) = 5 Å and σ_{vdW} (toluene) = 5.5 Å. The broadening of the transition can be as large as 40 K in MCM-41. See ref 28.

adiabatic calorimetry corresponds correlations times of 200 and 1000 s, T_g(NMR) is always larger than the glass transition temperature determined by calorimetric methods. Figure 11 displays the glass transition temperatures of confined benzene and toluene as a function of the ratio σ_{vdW}/d, where σ_{vdW} is the van der Waals diameter of the molecule and d the pore diameter. The glass transition temperature of confined benzene increases continuously with decreasing pore size. This behavior is different from that of toluene confined in the same porous materials as displayed on Figure 11.[28] Most of the studies on confined organic glass-forming compounds were carried out in hydrophobic porous materials.[53−56] In all cases, the dynamics of the confined fluid is faster than in the bulk, and a decrease of T_g with decreasing pore size was observed. This behavior may be interpreted as finite size effects. However, recent experiments on glass-forming liquids confined in weakly interacting porous materials showed that the pore size dependence of T_g may be more complicated. The ideas behind most of these studies were to probe the cooperative length involved in the glass transition, ξ. But by confining a system at the nanoscale, new parameters that may influence the behavior of the confined phases are introduced. First of all, the pore diameter d becomes a new parameter that can be changed. The molecular size σ is an additional parameter that must be considered. When comparing different systems, σ and d can be taken into account as a new parameter d/σ. Fluid−wall interactions induce the formation of an interfacial liquid of one or more layers. The excluded volume due to molecules slowed down in this interfacial layer should also be considered in the structural properties. Moreover, this interfacial layer introduces spatial inhomogeneities in the dynamical properties of the confined fluids. The presence of a rigid wall also induces a gradual slowdown of the molecules with respect to their distance to the wall.[56] A cooperative length, ξ_{conf}, intrinsic to the studied system can be extracted from this progressive slowdown. If the cooperative length associated with dynamical heterogeneities responsible for the viscous slowdown exists in the bulk liquid, it should be comparable to ξ_{conf}. However, this comparison can be made only if confinement does not significantly modify the density and the structural properties of the confined fluid. The issue is the qualitative and even quantitative determination of this length scale under confinement. We will show in the following that its determination requires conditions that can rarely all be met. First, we will discus the choice of the liquid to confine. Fragile liquids are the best candidates for easy observation of finite size effects under confinement, because they exhibit super-Arrhenian behavior with pronounced variations of the relaxation times on cooling. Any deviation from this behavior under confinement should lead to an important gradient of the dynamics inside the pores and should be more easily detected. However, as experimental measurements are averaged over the molecules, these effects can only be observed if the fraction of fast molecules is not negligible compared to the fraction of slow molecules. For this condition to be fulfilled, the pore diameter should be carefully chosen: if the pore size is too small, the fraction of slow molecules is too important, and if it is too large, the dynamics at the center of the pore will be the same as that of the bulk. In both cases, finite size effects cannot be observed. The appropriate pore size to observe finite size effects is 2 to 3 ξ_{coop} (condition 1). Fluid−wall interactions should also be minimized in order to limit the amplitude of the perturbation caused by the rigid wall. The fraction of the slow molecules should be small enough so that $n_{slow} \times \tau_{slow}$ and $n_{fast} \times \tau_{fast}$ are of the same order of magnitude (condition 2). Postsynthesis modifications of the wall properties, silanization for instance, are a way to minimize fluid−wall interactions. To observe an important gradient of relaxation times, the experiments must be performed at low temperature close to T_g (condition 3). As the cooperative length is supposed to increase with decreasing temperature, the amount of fast molecules at the center of the pores also decreases. In the temperature range where the effects are maximal, the fraction of fast molecules is too small, condition 2 cannot be fulfilled, and ξ cannot be detected. Another important issue is the thermodynamic properties of confined fluids. To attribute the behavior of fragile liquids to finite size effects, their glass transition in confined geometry should be compared to that of the bulk liquid at the same density. The confined fluid may also be out of equilibrium even above its glass transition temperature. Under confinement, volume relaxation involves slow phenomena due to adsorption coupled with structural relaxation, and experimental observations correspond to a mixture of thermodynamic states at constant density and/or constant pressure.[57] However, if we consider that fragility is fundamental for a better understanding of glass transition and that the understanding of different behavior may lead to universal features, it is interesting to compare the properties of confined liquids. Here, we compare fragile and intermediate systems. Toluene is a fragile liquid and, even if bulk benzene usually crystallizes, it is supposed to behave as an intermediate Lennard-Jones liquid. The sizes of two molecules are similar, and they have the same types of interactions with the porous materials walls: their ratios σ/d are on the same order of magnitude when confined in the same materials. The same experiments were performed to study the two systems. Their behavior can then be compared in the same conditions. The

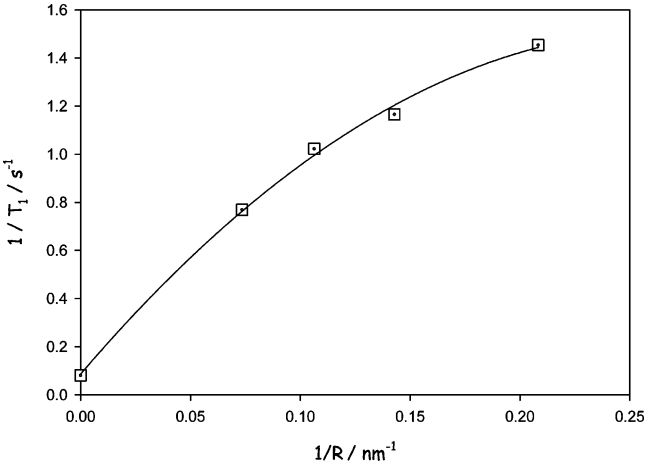

Figure 12. Proton spin−lattice relaxation time as a function of the reverse pore size at 298 K.

differences observed in their behaviors may be correlated to their fragilities.

All the transitions of confined benzene are summarized in a temperature−pore diameter (T, d) diagram (Figure 10). T_g of benzene confined in microemulsion, reported by Dubochet, was added to the graph.[14] To avoid crystallization, the sample was quenched to 100 K. On heating, the glass transition occurred at 118 K, followed by crystallization at 193 K and melting at 267 K. This behavior is typical of a glass-forming liquid in its bulk form. As the micelle sizes in these experiments are around 40σ, T_g in the microemulsion may be considered as the bulk limit. It is important to notice that, for benzene confined in MCM-41, the phenomenology is different: confined benzene vitrifies at the usual cooling rates, whereas vitrification is obtained only by quenching the sample in the microemulsion. Moreover, no crystallization is observed on heating above T_g for benzene confined in MCM-41.

The phase diagram may be divided into three parts representing the liquid, the crystal, and the glass domains. These domains are separated by the transition lines. Changing the properties of the porous material surface should lead to a shift or even a change in the shape of the transition lines. This is illustrated by the melting line of benzene confined in hydrophobic CPG from the experiments of Jackson and McKenna. Shifts of the transition line may come from the differences in the surface properties or topology. The determination of the respective parts of these two parameters requires more studies. Watanabe and Kaneko observed an increase of melting temperature for benzene confined in strongly attractive ACFs, even in very small pores.[15] The larger the pore, the larger the temperature shift is. In this case, both the surface properties of the materials and the shape of the pore seem important.

IV. 2. Dynamics. Geometrical confinement and surface interactions may be responsible for the slowdown of the dynamics, which causes an enhancement of the spin−spin and spin−lattice relaxation rates. To determine the respective parts of geometrical confinement and surface interactions effects in the decrease of spin−lattice relaxation times of confined benzene in the liquid phase, we applied the model proposed by Jonas and co-workers to our data at 298 K (Figure 12).[58−60] They studied a series of liquids confined in porous materials with weak or strong surface interactions. Using the two-phase fast exchange mechanism to treat the surface interactions and the fact that the spin−lattice relaxation rate of confined molecules depends on the bulk relaxation time T_{1b} and the surface one T_{1s}, they established the following expression for T_{1conf}:

$$\frac{1}{T_{1\mathrm{conf}}} = \frac{1}{T_{1\mathrm{b}}} + \frac{2\epsilon}{R}\left(\frac{1}{T_{1\mathrm{s}}} - \frac{1}{T_{1\mathrm{b}}}\right) - \frac{\epsilon^2}{R^2}\left(\frac{1}{T_{1\mathrm{s}}} - \frac{1}{T_{1\mathrm{b}}}\right) + \frac{A(\omega)}{R^2}$$

T_{1b} and T_{1s} are, respectively, the bulk and the surface layer relaxation rates, R is the pore radius, ϵ the thickness of the surface layer, and $A(\omega)$ represents the topological confinement. This expression supports two limiting behaviors: $1/T_{1conf} \propto 1/R$ when the adsorbed liquid has a strong interaction with the pore surface and $1/T_{1conf} \propto 1/R^2$ for the weak interacting liquids. Figure 12 displays the relaxation rate of confined benzene versus $1/R$ at 298 K. We fit our data with the following equation: $1/T_1 = 1/T_{1b} + a/R^2 + b/R$ (eq 1) where $a = \epsilon(1/T_{1s} - 1/T_{1b})$ and $b = A(\omega) - \epsilon^2(1/T_{1s} - 1/T_{1b})$. If the nuclear relaxation rates depend only on topological effects, $a \gg b$, as found by Korb et al. for methylcyclohexane confined in modified porous silica with nonpolar groups at the surface ($a = 73.0$ and $b = 0.78$).[46] In the case of strongly interacting liquids, the nuclear relaxation is dominated by surface relaxation and $a \ll b$, as for nitrobenzene confined in nonmodified silica gel ($a = 0$ and $b = 4.11$) or polar molecules such as ethanol or trifluoroethanol confined in porous silica.[48,58] In this case, the relaxation rate has a linear dependence on $1/R$. The best fit of our data gives the following values for the constants: $a = 10.7 \pm 0.9$ and $b = -19.9 \pm 3.0$. The fact that the two constants are on the same order of magnitude indicates that, in the case of a van der Waals liquid such as benzene, both surface interaction and geometrical confinement are at the origin of the enhancement of the relaxation rate. These results also show that interactions between benzene and the silica walls are strong and are in agreement with the results of Zhu on the dynamics of confined benzene.[46] The evolutions of T_1 as a function of temperature in the bulk and in confined geometry are very different. The activation energies calculated for all the confined samples are equal, suggesting that the relaxation mechanism is the same in all the samples. Its value ($\sim$8 kJ.mol^{-1}) is close to the activation energy of 3.4 kJ.mol^{-1} for the reorientation about the C_6 axis determined by Witt et al. with ^{13}C NMR.[60] The activation energies of confined samples are lower than that of bulk crystalline benzene (15.5 kJ.mol^{-1}). This can be explained by the fact that a non-negligible amount of liquid exists in the samples in the whole temperature range. Moreover, the confined crystal may be highly defective, particularly in nanopores. In his experiments on confined liquid benzene, Zhou showed that benzene molecules lie flat on the pore surfaces, and these effects persist over large distances leading to the structuring of the liquid. This structuring may explain why the relaxation mechanisms of the liquid and the crystal are the same. These results are also in agreement with the experiments of Yi and Jonas, who showed that rotation of benzene confined in nanoporous silica glass becomes anisotropic under confinement, with a parallel diffusion constant larger than the perpendicular diffusion one.

V. Conclusion

We present here the first complete (d, T) phase diagram of benzene confined in silica-walled MCM-41 and SBA-15 showing the transition temperatures as a function of pore size. Even if the benzene molecule strongly wet silica as reported in the literature, its behavior is different from that of water under confinement.[12,46] In SBA-15, a decrease of the melting temperature is always observed. The comparison of the freezing and melting behavior with experiments in ACF or hydrophobic CPG show that phase behavior of benzene confined in these materials is strongly influenced by fluid−wall interactions.

However, the topologies of ACF (confinement in one dimension) and CPG (confinement in two dimensions, interconnected pores) differ from those of MCM-41 and SBA-15 (confinement in two dimensions). Neutron diffraction measurements showed that, for benzene, the structures of the liquid or the crystal are not noticeably changed under confinement. Proton NMR spin−spin and spin−lattice relaxation times show a slowdown of the overall dynamics of the confined phases compared to the bulk. Unlike bulk benzene, in the partially crystallized samples, the spin−lattice relaxation times of the liquid layer and that of the crystal are equal, indicating that reorientation motion mechanisms are identical in both phases. Our results were obtained in rigid confinement; the dynamical properties show that benzene strongly interacts with silica. To be able to go further in the understanding of fluid−wall interaction effects at constant topology, it is important to increase or decrease fluid−wall interactions. Cylindrical nanoporous materials with carbon walls, which will interact more strongly than silica with benzene, would be useful to extract the pore topology role in the behavior of the confined phases. Soft confinement conditions appear in numerous areas such as life sciences. Recent results from Richert and collaborators on the dynamics of a glass-forming liquid in soft confinement displays faster dynamics than the bulk liquid.[62] Experiments in soft confinement are the next step for a better understanding of phase behavior, structure, and dynamical properties of phases in these conditions.

References and Notes

(1) Gelb, D. L.; Gubbins, K. E.; Radhakrishnan, R.; Sliwinska-Bartkowiak, M. *Rep. Prog. Phys.* **1999**, *62*, 1573−1659.

(2) Büttner, H., Zorn, R., Eds. 1st International Workshop on Dynamics in Confinement. *J. Phys. IV* **2000**, 10.

(3) Frick, B., Koza, M., Zorn, R., Eds. 2nd International Workshop on Dynamics in Confinement. *Eur. Phys. J. E* **2003**, 12.

(4) Christenson, H. K. *J. Phys.: Condens. Matter* **2001**, *13*, 95.

(5) Alcoutlabi, M.; McKenna, G. B. *J. Phys.: Condens. Matter* **2005**, *17*, R461.

(6) Alba-Simionesco, C.; Coasne, B.; Dosseh, G.; Dudziak, G.; Gubbins, K. E.; Radhakrishnan, R.; Sliwinska-Bartkowiak, M. *J. Phys.: Condens. Matter* **2006**, *18*, R15.

(7) Jackson, C. L.; McKenna, G. B. *J. Chem. Phys*. **1990**, *93*, 9002.

(8) Jackson, C. L.; McKenna, G. B. *Chem. Mater*. **1996**, *8*, 2128.

(9) Mu, R.; Malhotra, V. M. *Phys. Rev. B* **1991**, *44*, 4296.

(10) Radhakrishnan, R.; Gubbins, K. E.; Sliwinska-Bartkowiak, M. *J. Chem. Phys*. **2000**, *112*, 11048.

(11) Radhakrishnan, R.; Gubbins, K. E.; Sliwinska-Bartkowiak, M. *J. Chem. Phys*. **2002**, *116*, 1147.

(12) Dosseh, G.; Xia, Y.; Alba-Simionesco, C. *J. Phys. Chem. B* **2003**, *107*, 6445.

(13) Morishige, K.; Kawano, K. *J. Chem. Phys*. **1999**, *110*, 4867.

(14) Dubochet, J.; Adrian, M.; Teixeira, J.; Alba, C. M.; Kadiyala, R. K.; MacFarlane, D. R.; Angell, C. A. *J. Phys. Chem*. **1984**, *88*, 6727.

(15) Watanabe, A.; Kaneko, K. *Chem. Phys. Lett*. **1999**, *305*, 71.

(16) Sliwinska-Bartkowiak, M.; Dudziak, G.; Sikorski, R.; Gras, R.; Radhakrishnan, R.; Gubbins, K. E. *J. Chem. Phys*. **2001**, *114*, 950.

(17) Israelachvili, J. N.; McGuiggan, P. M.; Homola, A. M. *Science* **1988**, *240*, 189.

(18) Klein, J.; Kumacheva, E. *J. Chem. Phys.* **1998**, *108*, 6996.

(19) Carson, G. A.; Granick, S. *Phys. Rev. Lett.* **1991**, *66*, 2758.

(20) Granick, S. *Science* **1991**, *253*, 374.

(21) Raviv, U.; Laurat, P.; Klein, J. *Nature (London)* **2001**, *413*, 51.

(22) Raviv, U.; Giasson, S.; Frey, J.; Klein, J. *J. Phys.: Condens. Matter* **2002**, *14*, 9275.

(23) Radhakrishnan, R.; Sliwinska-Bartkowiak, M.; Gubbins, K. E.; Watanabe, A.; Kaneko, K. *J. Chem. Phys.* **1999**, *111*, 9058.

(24) Sliwinska-Bartkowiak, M.; Gras, R.; Sikorski, R.; Radhakrishnan, R.; Gelb, L.; Gubbins, K. E. *Langmuir* **1999**, *15*, 6060.

(25) Booth, H. F.; Strange, J. H. *Mol. Phys.* **1998**, *93*, 263.

(26) Morishige, K.; Kawano, K. *J. Chem Phys.* **2000**, *112*, 11023.

(27) Asknes, D. W.; Gjerdåker, L. *J. Mol. Struct.* **1999**, *475*, 27.

(28) Morineau, D.; Xia, Y.; Alba-Simionesco, C. *J. Chem. Phys*. **2002**, *117*, 8966.

(29) Teboul, V.; Alba Simionesco, C. *J. Phys.: Condens. Matter* **2002**, *14*, 5679.

(30) Korb, J. P.; Xu, S.; Jonas, J. *J. Chem. Phys*. **1993**, *98*, 2411.

(31) Arndt, M.; Stannarius, R.; Gorbatschow, W.; Kremer, F. *Phys. Rev. E* **1997**, *54*, 5377.

(32) Zorn, R.; Frick, B.; Kremer, F.; Schönhals, A.; Hartman, L.; Richter, D. *Physica B* **2004**, *350*, e1115.

(33) Frick, B.; Alba-Simionesco, C.; Dosseh, G.; Le Quellec, C.; Moreno, A. J.; Colmenero, J.; Schönhals, A.; Zorn, R.; Chrissopoulou, K.; Anastasiadis, S. H.; Dalnoki-Veress, K. *J. Non-Cryst. Solids*, accepted 2005.

(34) Loughane, B. J.; Farrer, R. A.; Scodinu, A.; Reilly, T.; Fourkas, J. T. *J. Phys. Chem. B* **2000**, *104*, 5421.

(35) Richert, R.; Min, Y. *J. Phys. Chem*. **2003**, *107*, 895.

(36) Craven, C. J.; Hatton, P. D.; Howard, C. J.; Pawley, G. S. *J. Chem. Phys*. **1993**, *98*, 8236. Craven, C. J.; Hatton, P. D.; Pawley, G. S. *J. Chem. Phys*. **1993**, *98*, 8244.

(37) Grün, M.; Lauer, I.; Unger, K. *Adv. Mater*. **1997**, *9*, 254.

(38) Morineau, D.; Dosseh, G.; Alba-Simionesco, C.; Llewellyn, P. *Philos. Mag. B* **1999**, *79*, 1847−1855.

(39) Zhao, D.; Feng, J.; Huo, Q.; Melosh, N.; Fredrickson, G. H.; Chmelka, B. F.; Stucky, G. D. *Science* **1998**, *279*, 548.

(40) Kruk, M.; Jaroniec, M.; Sayari, A. *Chem. Mater*. **1999**, *11*, 492.

(41) Barrett, E. P.; Joyner, L. G.; Halenda, P. P. *J. Am. Chem. Soc.* **1951**, *73*, 373.

(42) Morineau, D.; Alba-Simionesco, C. *J. Chem. Phys.* **1998**, *109*, 8494.

(43) Morineau, D.; Alba-Simionesco, C. *J. Chem. Phys.* **2003**, *118*, 9389.

(44) Massiot, D.; Fayon, F.; Capron, M.; King, I.; Le Calvé, S.; Alonso, B.; Durand, J. O.; Bujoli, B.; Gan Hoatson, Z. *Magn. Reson. Chem*. **2002**, *40*, 70−76.

(45) Guégan, R.; Morineau, D.; Loverdo, C.; Béziel, W. *Phys. Rev. E* **2006**, *73*, 011707.

(46) Zhu, X.; Farrer, R. A.; Fourkas, J. T. *J. Phys. Chem. B* **2005**, *109*, 12724.

(47) Gedat, E.; Schreiber, A.; Albrecht, J.; Emmler, Th.; Shenderovich, I.; Findenegg, G. H.; Limbach, H.-H.; Buntkowsky, G. *J. Phys. Chem. B* **2002**, *106*, 1977.

(48) Korb, J. P.; Delville, A.; Xu, S.; Demeulenaere, G.; Costa, P.; Jonas, J. *J. Chem. Phys* **1994**, *101*, 7074.

(49) Bloembergen, N.; Purcell, E. M.; Pound, R. V. *Phy. Rev*. **1948**, *73*, 679.

(50) Kubo, R.; Tomita, K. *J. Phys. Soc. Jpn.* **1954**, *9*, 888.

(51) Yi, J.; Jonas, J. *J. Phys. Chem.* **1996**, *100*, 16789.

(52) Cox, E. G. *Rev. Mod. Phys.* **1958**, *30*, 159.

(53) Jackson, C. L.; McKenna, G. B. *J. Non-Cryst. Solids* **1991**, *131*−*133*, 221.

(54) Arndt, M.; Stannarius, R.; Groothues, H.; Hempel, E.; Kremer, F. *Phys. Rev. Lett.* **1997**, *79*, 2077.

(55) Schönhals, A.; Goering, H.; Schick, Ch. *J. Non-Cryst. Solids* **2002**, *305*, 140.

(56) Scheidler, P.; Kob, W.; Binder, K. *Eur Phys. J. E* **2003**, *12*, 5.

(57) Yan, X.; Streck, C.; Richert, R. *Ber. Bunsen-Ges. Phys. Chem.* **1996**, *100*, 1392.

(58) Korb, J. P.; Xu, S.; Jonas, J. *J. Chem. Phys* **1993**, *98*, 2411.

(59) Ballard, L.; Jonas, J. *Langmuir* **1996**, *12*, 2798.

(60) Sullivan, V. S.; Kim, Y. J.; Xu, S.; Jonas, J.; Korb, J. P. *Langmuir* **1999**, *15*, 4664.

(61) Witt, R.; Sturz, L.; Doelle, A.; Mueller-Plathe, F. *J. Phys. Chem. A* **2000**, *104*, 5716.

(62) Wang, L.-M.; He, F.; Richert, R. *Phys. Rev. Lett*. **2004**, *92*, 095701.